Journal of Alloys and Compounds 509 (2011) 9479–9486

Contents lists available at ScienceDirect

Journal of Alloys and Compounds

journal homepage: www.elsevier.com/locate/jallcom

Synthesis and photocatalytic performance of Ag-loaded β-Bi_2O_3 microspheres under visible light irradiation

Gangqiang Zhu, Wenxiu Que*, Jin Zhang

Electronic Materials Research Laboratory, School of Electronic and Information Engineering, Xi'an Jiaotong University, Xi'an 710049, Shaanxi, PR China

ARTICLE INFO

Article history:
Received 17 June 2011
Received in revised form 12 July 2011
Accepted 16 July 2011
Available online 22 July 2011

Keywords:
Photocatalyst
Microspheres
Photoluminescence
Visible light irradiation

ABSTRACT

The visible-light-driven photocatalyst Ag/β-Bi_2O_3 microspheres were synthesized by a simple chemical method. First, β-Bi_2O_3 microspheres were obtained by a thermal treatment of sphere-like $Bi_2O_2CO_3$ precursor at 360 °C for 3 h in air and then Ag nanoparticles were in situ incorporated into β-Bi_2O_3 microspheres by impregnation method. The as-synthesized samples were characterized by X-ray powder diffraction (XRD), scanning electron microscopy (SEM), transmission electron microscopy (TEM), X-ray photoelectron spectroscopy (XPS), UV–vis spectroscopy and photoluminescence measurements. The experimental results demonstrated that the visible light absorption of β-Bi_2O_3 photocatalyst is greatly enhanced with the incorporation of Ag nanoparticles. The SEM and TEM observations revealed that the Ag nanoparticles can be homogenously incorporated in the β-Bi_2O_3 microspheres. The photocatalytic activity of Ag/β-Bi_2O_3 sample was evaluated by the photodegradation of the Rhodamine-B under visible light irradiation as a function of Ag content. It is found that the photocatalytic efficiency of β-Bi_2O_3 can be significantly improved with the incorporation of Ag nanoparticles up to 2.0 wt% Ag. The mechanism for the enhanced photocatalytic activity is also presented.

1. Introduction

Since the photoinduced decomposition of water on TiO_2 electrodes has been discovered, semiconductor-based photocatalysis for the degradation of organic compounds has been attracting an extensive research interest in the past twenty years [1]. Particularly, TiO_2 photocatalytic disinfection has been intensively studied due to its safety, low-cost and efficiency [2]. Because of its wide band gap (ca. 3.2 eV), low quantum yield and the absorbance of only near UV-region (λ < 400 nm) limit its practical applications. In order to extend its photosensitivity to visible region, TiO_2 has been doped with various non-metal and metal atoms, such as nitrogen [3], fluorine [4], iron [5] and vanadium [6]. Nevertheless, these dopants may also act as a recombination center among photo-generated carriers, which is usually discrete and inconvenient for the migration of the electrons and holes. Therefore, it is essential to develop efficient visible-light-active photocatalysts that can be used under solar irradiation.

Bismuth oxide (Bi_2O_3) is an important p-type semiconductor with four main crystallographic polymorphs denoted as α-, β-, γ-, and δ-Bi_2O_3 [7]. Due to unique optical and electrical properties, Bi_2O_3 has been extensively investigated for various applications in gas sensors, photovoltaic cells, optical coatings, fuel cells, supercapacitors, photocatalysts, etc. [7–9]. The band gap of Bi_2O_3 (2.58–2.85 eV) is narrower than that of the TiO_2, which is the most widely used and traditional photocatalyst. Bi_2O_3 has been studied as a visible-light-driven photocatalyst [10–13]. The intrinsic polarizability induced by the Bi $6s^2$ lone pairs of electron is helpful for the separation of the photogenerated electron–hole pairs and the transfer of the charge carriers [14]. However, the photocatalytic activity of Bi_2O_3 is low due to the fast recombination of the photogenerated electron–hole pairs [15]. Therefore, the photodegradation efficiency of Bi_2O_3 catalyst needs to be further improved. In recent years, noble metal and semiconductor-based heterogeneous catalytic ozonation has been receiving considerable attention due to its potentially greater effectiveness in the degradation and the mineralization of harmful organic pollutants with lower negative effects [16,17]. Thus, the nanostructured metals were used to improve the generation of electron-rich species, such as O^-, $O_2^{\bullet -}$, $HO_2^\bullet$ and $^\bullet OH$, during the ozonation treatment [16–18]. Additionally, the nano-sized metals, as catalysts, exhibit a pronounced enhancement in catalytic activity owing to the enhanced surface to volume ratio and quantum-size effect [18,10]. Since the metal nanoparticles can store electrons making the e^-/h^+ charge separation [19], the catalytic activity was found to be more enhanced when noble metals, such as Au, Ag, Cu and Pt nanoparticles, were loaded on the semiconductors. Although some works have been done on the heterogeneous

* Corresponding author at: Electronic Materials Research Laboratory, School of Electronic and Information Engineering, Xi'an Jiaotong University, 28 Xianning West Road, Xia'n 710049, Shaanxi, PR China. Tel.: +86 29 82668679; fax: +86 29 82668794.
E-mail address: wxque@mail.xjtu.edu.cn (W. Que).

0925-8388/$ – see front matter © 2011 Elsevier B.V. All rights reserved.
doi:10.1016/j.jallcom.2011.07.046

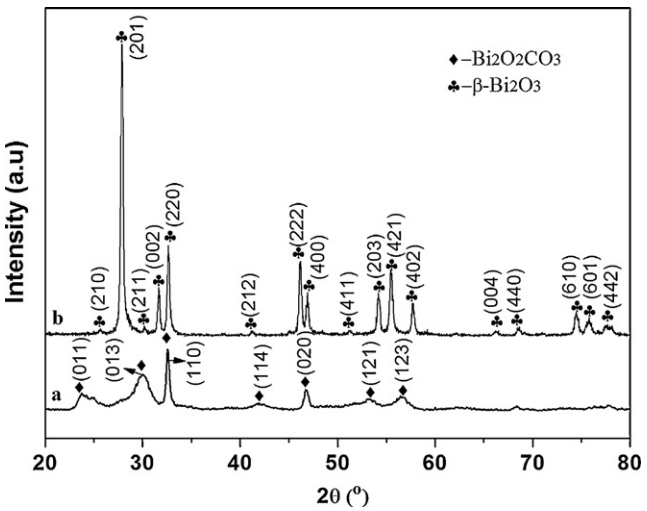

Fig. 1. XRD patterns of the as-prepared $Bi_2O_2CO_3$ (a) and β-Bi_2O_3 (b).

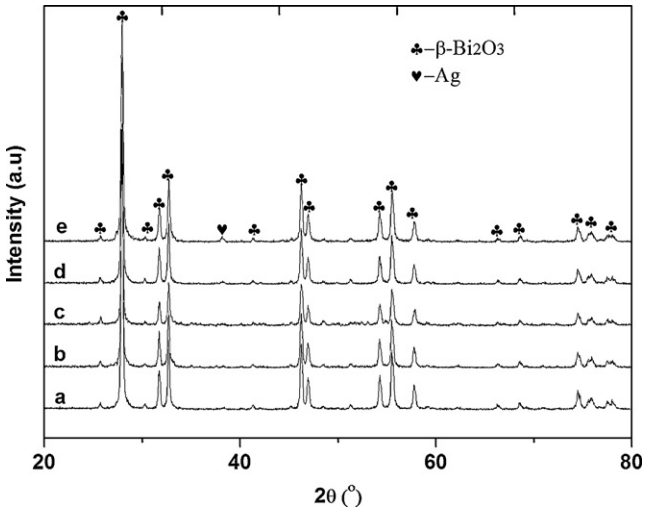

Fig. 3. XRD patterns of Ag/β-Bi_2O_3 sample as a function of Ag content: 0.5 wt% (a), 1.0 wt% (b), 2.0 wt% (c), 3.0 wt% (d) and 4.0 wt% (e).

catalytic activities of the noble metals loaded α-Bi_2O_3 nanostructures [20–22], the photocatalytic activity of the composites is still inefficient. It is therefore of interesting to investigate the photocatalytic activity of noble metals loaded β-Bi_2O_3 nano- and microstructures.

Here, we emphasize on the synthesis and photocatalytic activity of Ag nanoparticles loaded β-Bi_2O_3 microspheres. The photocatalytic activity of Ag/β-Bi_2O_3 photocatalyst was evaluated by the degradation of Rhodamine-B (RhB) under visible light irradiation, and the mechanism of the enhanced photocatalytic activity is also presented.

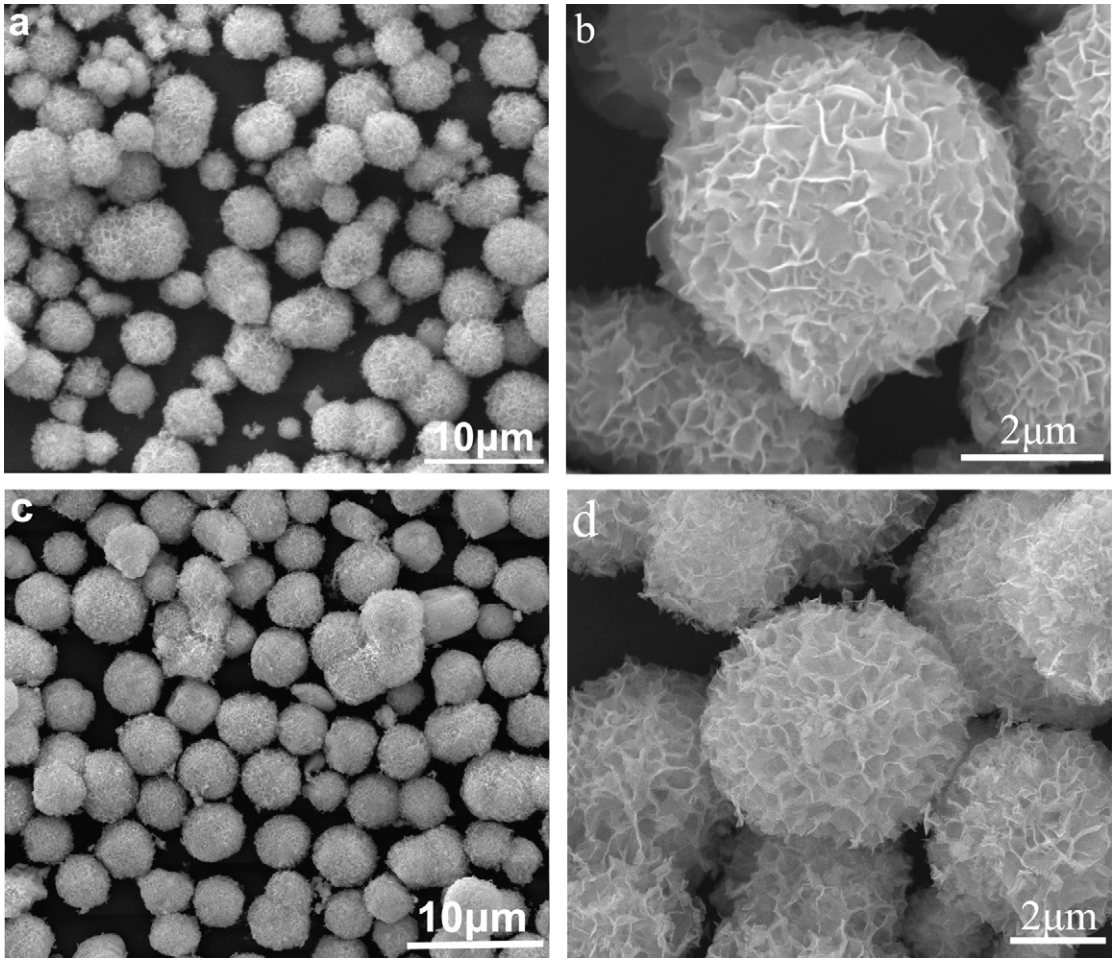

Fig. 2. SEM micrographs of the as-prepared $Bi_2O_2CO_3$ (a and b) and β-Bi_2O_3 (c and d).

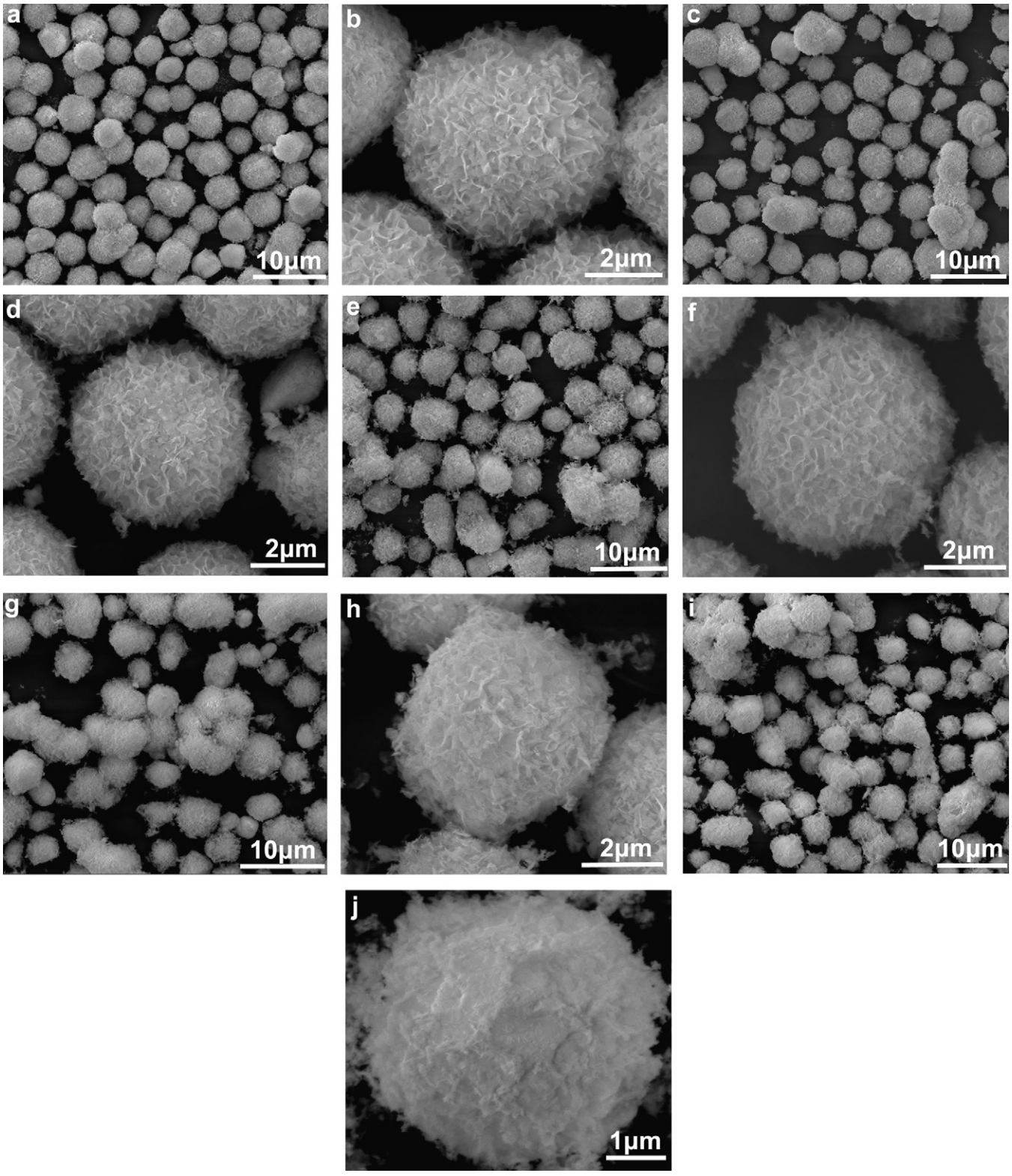

Fig. 4. SEM micrographs of Ag/β-Bi_2O_3 sample as a function of Ag content: 0.5 wt% (a and b), 1.0 wt% (c and d), 2.0 wt% (e and f), 3.0 wt% (g and h) and 4.0 wt% (i and j).

2. Experimental

2.1. Synthesis

All chemical reagents purchased from Shanghai Chemical Reagent Co., China, were of analytical grade and used without further purification. β-Bi_2O_3 microspheres were obtained by a thermal treatment of sphere-like $Bi_2O_2CO_3$ precursor. Hence, the sphere-like $Bi_2O_2CO_3$ precursor was firstly synthesized by a hydrothermal method [23]. In a typical procedure to prepare sphere-like $Bi_2O_2CO_3$ precursor, 2 mmol of $Bi(NO_3)_3{\cdot}5H_2O$ was dissolved in 10 mL of 1 M HNO_3, and then 1.5 mmol of citric acid was introduced into the solution. After being magnetically stirred for 10 min, the pH value of the clear solution was adjusted to 4 with the addition of 2 M NaOH solution under vigorous stirring. The formed white-colored precursor was transferred into a Teflon-lined stainless steel autoclave and maintained at 180 °C for 24 h. After cooling the hydrothermal system to room temperature, the sphere-like $Bi_2O_2CO_3$ precursor was separated by a centrifugation process, washed

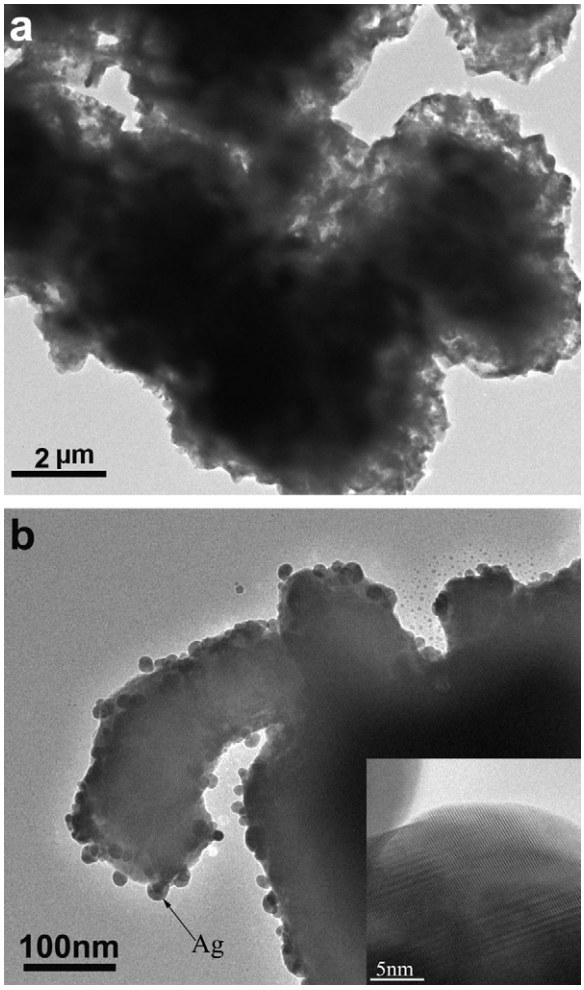

Fig. 5. TEM (a and b) and HRTEM (inset) micrographs of Ag/β-Bi_2O_3 sample with 2.0 wt% Ag.

with distilled water and absolute ethanol for several times, and dried under vacuum at 80 °C for 5 h. The as-prepared sphere-like $Bi_2O_2CO_3$ precursor was then heat treated at 360 °C for 3 h in air in order to obtain β-Bi_2O_3 microspheres. The incorporation of Ag nanoparticles (0.5–4 wt%) into β-Bi_2O_3 microspheres was performed by impregnation method. First, 1 g of the as-prepared β-Bi_2O_3 powder was placed in a glass beaker and then 1 mL of aqueous solution of $AgNO_3$ was added. The beaker was placed in a water bath, and the suspension was manually stirred using a glass rod during the evaporation of water. For the complete decomposition of NO_3^- ions, the dried sample from the water bath was further heated using the Bunsen burner. Finally, a low temperature reduction treatment of the sample was performed at 80 °C for 1 h under a steady flow of hydrogen gas.

2.2. Characterization

The phase compositions and crystal structures of the as-synthesized samples were determined by X-ray powder diffraction (XRD) using a D/Max2550 diffractometer (Rigaku, Japan) at a scanning rate of 5° min^{-1} in the 2θ range from 10° to 70°, with Cu Kα radiation (λ = 1.5406 Å) at 40 kV and 50 mA. The morphologies of the as-synthesized samples were examined using a Quanta 200 scanning electron microscope (FEI, The Netherlands) equipped with an energy dispersive X-ray spectroscopy (EDS). Transmission electron microscopy (TEM) and high-resolution transmission electron microscopy (HRTEM) observations were performed using a JEM-2100F (JEOL, Japan) instrument at an accelerating voltage of 200 kV. The chemical states of elements in the samples were analyzed by X-ray photoelectron spectroscopy (XPS) using a VG ESCALAB MKII X-ray photoelectron spectrometer (VG Scienta, USA) with Mg Kα radiation. The optical properties of the samples were characterized by a photoluminescence (PL) measurement using a He–Cd laser (3.82 eV, 325 nm) as the excitation source at room temperature. The diffuse reflectance absorption spectra (DRS) of the samples were recorded on a Lambda 950 UV-VIS-NIR spectrophotometer (Perkin-Elmer, USA) in the range of 200–800 nm.

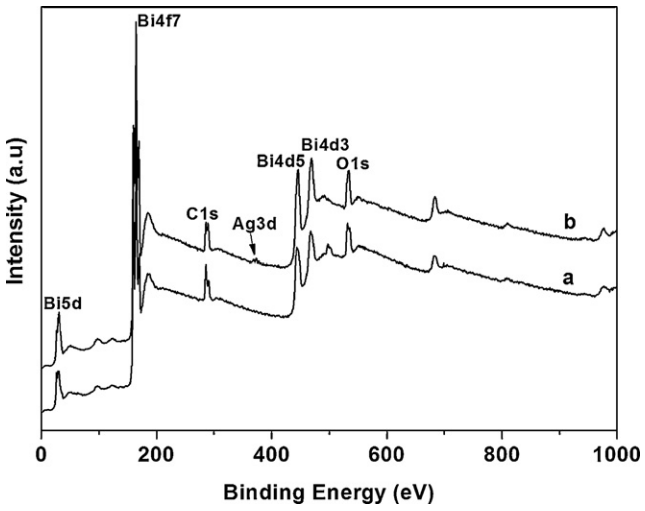

Fig. 6. XPS spectra of β-Bi_2O_3 (a) and Ag/β-Bi_2O_3 with 2.0 wt% Ag (b).

2.3. Photocatalytic activity

The photocatalytic activity of Ag/β-Bi_2O_3 sample was evaluated by the degradation of Rhodamine-B (RhB) under visible light irradiation (λ > 420 nm). The visible light was obtained by a 400 W halogen–tungsten lamp with a 420 nm cutoff filter to ensure that the desired irradiation light was obtained. The reaction temperature was maintained at 25 °C by cooling water in the cooling jacket of the reactor. The initial concentration of the RhB was 10 mg/L and the catalyst was 1.0 g/L. Prior to irradiation, the suspension was sonicated for 10 min and then magnetically stirred in the dark for 30 min to reach adsorption–desorption equilibrium between the RhB and the photocatalyst. During visible light irradiation, 2 mL of aliquots was sampled at certain time interval and centrifuged to remove solid particles. The filtrates were analyzed by recording variations in the absorption band at 533 nm in the UV–vis spectra of RhB by using a U-3010 UV–vis spectrophotometer (Hitachi, Japan).

3. Results and discussion

Fig. 1 shows the XRD patterns of the as-prepared $Bi_2O_2CO_3$ precursor before and after heat treatment at 360 °C for 3 h. Clearly, all diffraction peaks in the XRD pattern, shown in Fig. 1a, of the as-prepared $Bi_2O_2CO_3$ precursor before heat treatment are readily indexed to the hexagonal phase of bismuth subcarbonate ($Bi_2O_2CO_3$) with the lattice constants of $a = b = 3.868$ Å and $c = 13.673$ Å, which are in good agreement with the previously reported values (JCPDS card no. 41-1488). As for the as-prepared $Bi_2O_2CO_3$ precursor heat treated at 360 °C for 3 h, all the diffraction peaks in the XRD pattern (Fig. 1b) can be well indexed to the tetragonal phase of bismuth oxide (β-Bi_2O_3) with the lattice constants of $a = b = 7.740$ Å and $c = 5.632$ Å, which are consistent with the values from the standard JCPDS card no. 71-2274. This indicates that heat treatment at 360 °C for 3 h was favorable for the complete formation of β-Bi_2O_3 from the $Bi_2O_2CO_3$ precursor. The morphologies and microstructures of the as-prepared $Bi_2O_2CO_3$ precursor before and after heat treatment at 360 °C for 3 h were investigated with SEM and the results are illustrated in Fig. 2. It is visible from the SEM micrograph shown in Fig. 2a that the panoramic morphology of the as-prepared $Bi_2O_2CO_3$ precursor is spherical with an average diameter of ~5 μm. The magnified SEM micrograph in Fig. 2b reveals that each sphere is constructed by irregular nanosheets and has a porous-like structure. Quite surprisingly, the morphology of the as-prepared $Bi_2O_2CO_3$ precursor was not affected by heat treatment at 360 °C for 3 h that induced the phase transformation from $Bi_2O_2CO_3$ to β-Bi_2O_3. As can be seen in Fig. 2c and d, the sphere-like structures with an average diameter of ~5 μm are retained with no significant changes. Probably, heat treatment temperature was not high enough to cause a morphological transformation of the as-prepared $Bi_2O_2CO_3$ precursor.

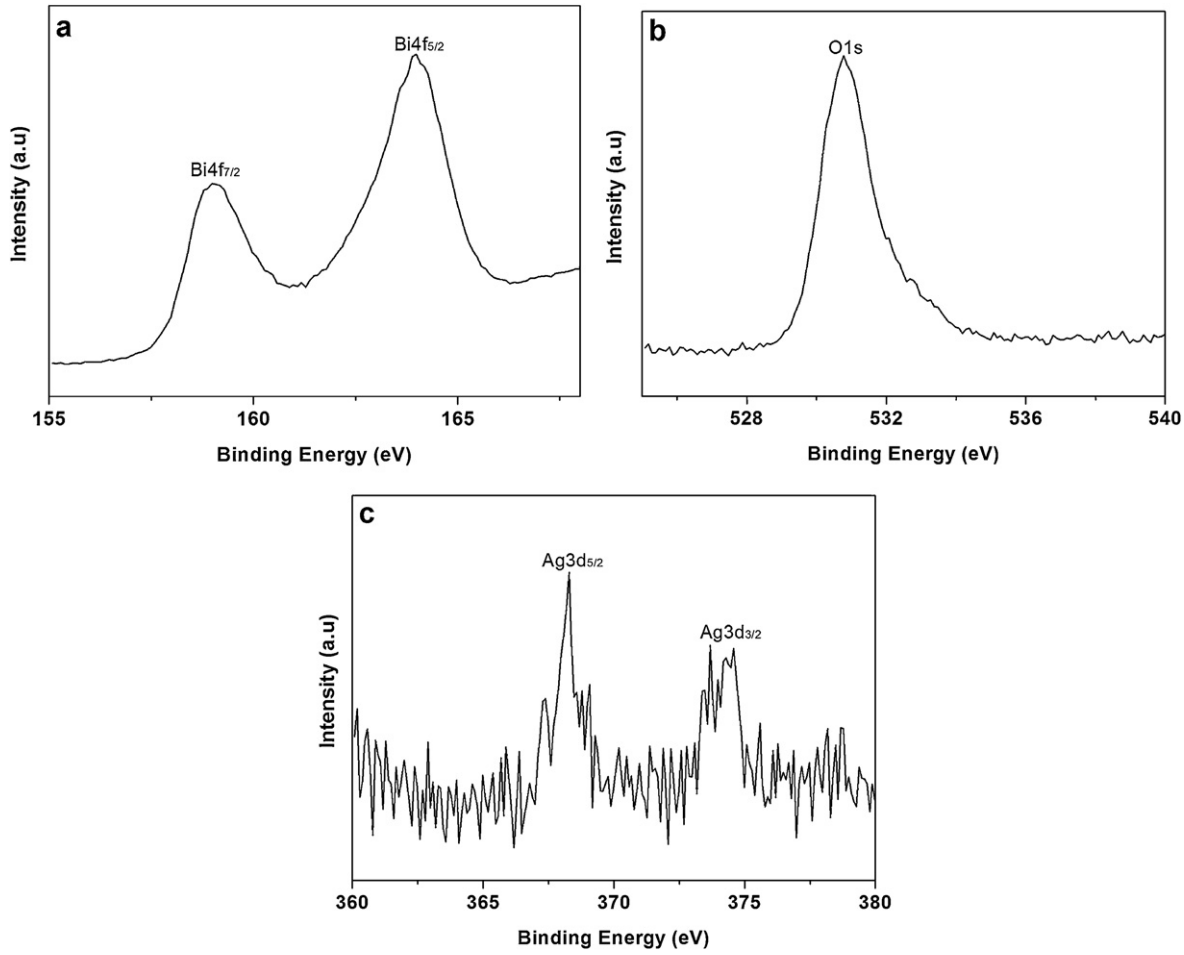

Fig. 7. XPS spectra of Ag/β-Bi_2O_3 sample with 2.0 wt% Ag: Bi 4f (a), O 1s (b) and Ag 3d (c).

The XRD patterns of Ag/β-Bi_2O_3 photocatalyst are shown in Fig. 3 as a function of Ag content. It is clearly indicated that all the samples doped with different Ag contents are well crystallized and exhibit sharp diffraction peaks corresponding to the tetragonal β-Bi_2O_3 (JCPDS card no. 71-2274). No phase transformation and no obvious change in the intensities of the diffraction peaks were noted with increasing Ag content. This means that the incorporation of Ag into β-Bi_2O_3 did not affect the crystal structure as well as crystallinity. Besides the strong reflections of β-Bi_2O_3, a weak diffraction peak at $2\theta = 38$, corresponding to the cubic phase of Ag (JCPDS card no. 04-0783), can be also seen for β-Bi_2O_3 samples loaded with 3–4 wt% Ag.

The morphologies of Ag/β-Bi_2O_3 samples were examined by SEM and TEM. Fig. 4 depicts the SEM micrographs of Ag/β-Bi_2O_3 sample as a function of Ag content. It can be seen from Fig. 4a and c that the Ag/β-Bi_2O_3 samples loaded with 0.5 wt% Ag and 1.0 wt% Ag have sphere-like structures with the diameter of ~5 μm; in addition, the surfaces of microspheres in Fig. 4b and d present porous-like structure. However, the shape of the sphere-like structure becomes non-uniform with increasing the Ag content to 2–4 wt% added into the β-Bi_2O_3, as shown in Fig. 4e–j. Also, the surface feature was negligibly changed with the increase in Ag content. Furthermore, in order to confirm the results obtained by SEM, the samples were examined by TEM observation. The TEM and HRTEM micrographs of Ag/β-Bi_2O_3 sample with 0.5 wt% Ag are shown in Fig. 5. These TEM micrographs also demonstrate that the morphology of the sample is sphere-like with the diameter of ~5 μm. It is visible from Fig. 5b that some tiny nanoparticles of Ag with the size of ~10–20 nm are attached onto the surface of the β-Bi_2O_3 microsphere. The HRTEM micrograph in an inset of Fig. 5b reveals the presence of Ag on the surface of the β-Bi_2O_3 microsphere. From the TEM and SEM observations, we can conclude that a higher Ag content slightly altered the shape and surface feature of the β-Bi_2O_3 microspheres.

To elucidate the elemental composition and the chemical state of Bi and Ag, the as-prepared samples were analyzed by X-ray photoelectron spectroscopy (XPS). Fig. 6 shows the typical XPS spectra for the as-prepared β-Bi_2O_3 and Ag/β-Bi_2O_3 loaded with 2.0 wt%. As can be seen, both samples show the presence of bismuth (Bi 4f, Bi 4d, Bi 4p, Bi 5d), oxygen (O 1s) and carbon (C 1s), and only the Ag-loaded Bi_2O_3 sample represents the Ag3d peak around 370 eV. Further, Fig. 7 shows the high-resolution XPS spectra of the three primary elements of the Ag/β-Bi_2O_3 sample loaded with 2.0 wt% Ag. In Fig. 7a and b, the binding energies of Bi $4f_{7/2}$, Bi $4f_{5/2}$, and O 1s are 159.0, 164.0 and 528.0 eV, respectively. Fig. 7c shows that the peaks of Ag $3d_{5/2}$ and Ag $3d_{3/2}$ are centered at 368.0 and 374.0 eV, respectively, which indicate that the state of Ag in the sample is metallic [24]. Surface elemental analysis reveals that the atomic ratio of Ag:Bi is 1:40. This value is higher than the theoretical one, which means that the Ag nanoparticles are well dispersed on the surface of β-Bi_2O_3 microspheres.

The color of Ag/β-Bi_2O_3 sample with low Ag content was yellowish brown and became completely brown with high Ag content. As one knows, the optical property of a semiconductor is related to its electronic structure and is recognized as a key factor in determining photocatalytic ability. The UV–vis absorption spectra of Ag/β-Bi_2O_3

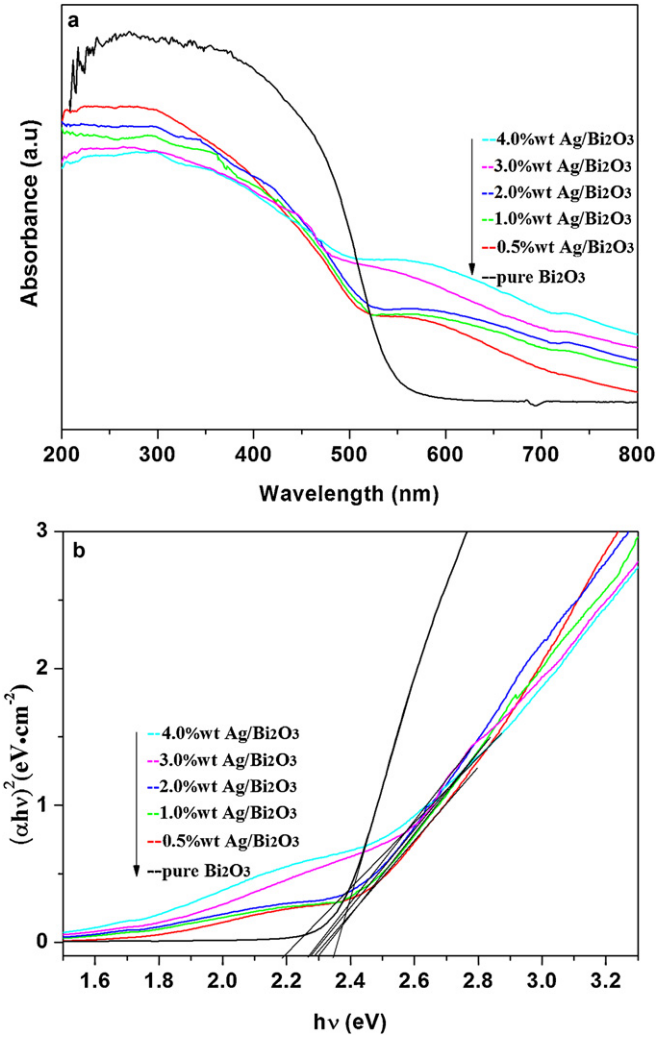

Fig. 8. UV–vis absorbance spectra (a) and plot of $(\alpha h\nu)^2$ versus $h\nu$ (b) of Ag/β-Bi_2O_3 sample as a function of Ag content.

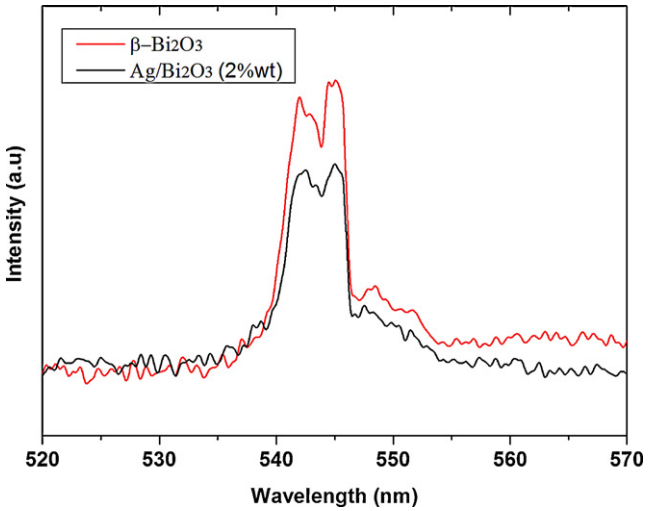

Fig. 9. PL spectra of β-Bi_2O_3 and Ag/β-Bi_2O_3 with 2.0 wt% Ag.

sample are shown in Fig. 8a as a function of Ag content. It is evident that pure β-Bi_2O_3 and Ag/β-Bi_2O_3 samples loaded with different Ag contents have a strong ultraviolet as well as visible light absorption in the range of 200–550 nm, indicating that the as-prepared samples have a strong visible light response. Especially, the visible light absorption of Ag/β-Bi_2O_3 samples is significantly enhanced and the absorption edge shifts to red light with the loading of Ag. For a crystalline semiconductor, it was shown that the optical absorption near the band edge follows the equation [25]:

$$\alpha h\nu = A(h\nu - E_g)^{n/2}$$

where α, ν, E_g and A are the absorption coefficient, the light frequency, the band gap, and a constant, respectively. According to this equation, the value of n is equal to 1. A plot of $(\alpha h\nu)^2$ versus $h\nu$ of Ag/β-Bi_2O_3 sample are shown in Fig. 8b as a function of Ag content. The estimated optical band gap of Ag/β-Bi_2O_3 photocatalyst decreases in the following order according to the Ag content: 2.34 eV (0 wt%) < 2.30 eV (1.0 wt%) < 2.28 eV (0.5 wt%) < 2.28 eV (2.0 wt%) < 2.27 eV (3.0 wt%) < 2.22 eV (4.0 wt%).

Photoluminescence (PL) emission spectra are often used to examine the efficiency of charge carrier trapping and transfer as well as to understand the fate of the e^+/h^- pairs in semiconductor particles [26]. Fig. 9 shows the room-temperature PL emission spectra of the as-prepared β-Bi_2O_3 and Ag/β-Bi_2O_3 sample loaded with 2.0 wt% Ag. The PL spectra show two emission peaks at 541 and 544 nm, respectively. It can also be clearly seen that the β-Bi_2O_3 and the Ag/β-Bi_2O_3 sample loaded with 2.0 wt% Ag display an identical position and shape of those two peaks in the PL spectra. This behavior of the samples may be attributed to a radiative recombination process of the e^-/h^+ pairs [21]. However, an absolute luminescence intensity of Ag/β-Bi_2O_3 sample is comparatively lower than that of pure β-Bi_2O_3 sample. Probably, it is due to a low radiative recombination process caused by Ag nanoparticles incorporated into the β-Bi_2O_3. When Ag nanoparticles are present on the surface of β-Bi_2O_3 microspheres, the photo-excited e^- can easily be transferred from the conduction band to Ag nanoparticles and further leads to the e^-/h^+ charge separation that results in the reduction of combination rate. The results presented above conclude that Ag/β-Bi_2O_3 sample can be applied as an effective photocatalyst compared to pure β-Bi_2O_3 sample.

The photocatalytic activities of the as-prepared β-Bi_2O_3 and Ag/β-Bi_2O_3 samples were evaluated by the degradation of Rhodamine-B (RhB) under visible light irradiation. The temporal changes in the RhB concentration were monitored by examining the variations in maximal absorption in UV–vis spectra at 554 nm. For a comparison, a direct photolysis of the RhB and the degradation of the RhB over β-Bi_2O_3 sample were also performed under the identical conditions. Fig. 10a shows the concentration change of RhB under visible light irradiation at 554 nm as a function of Ag content. A blank sample proves that there is no obvious change in the RhB concentration with the absence of the photocatalyst. In contrast, the as-prepared β-Bi_2O_3 indicates a better photocatalytic activity (44%) in degradation of the RhB in 210 min. Nevertheless, pure β-Bi_2O_3 still has a poor photocatalytic activity for the degradation of the RhB, although there is a strong absorption in visible light region. Clearly, the photocatalytic performance of pure β-Bi_2O_3 is significantly improved with the incorporation of Ag nanoparticles. The decrease in the RhB concentration increases up to 64% in the presence of Ag/β-Bi_2O_3 sample loaded with 0.5 wt% Ag. That is to say, the Ag content was an important factor for a higher photocatalytic activity of Ag/β-Bi_2O_3 photocatalyst. Because the structure of Ag/β-Bi_2O_3 sample favors the migration of the electron–hole pairs, leading to a higher photocatalytic activity. The results from the photodecomposition experiments indicate that the photocatalytic activity of Ag/β-Bi_2O_3 sample can be considerably improved with increasing Ag content up to 2.0 wt%. The highest photodegradation (98%) of the RhB in 210 min was in Ag/β-Bi_2O_3 sample loaded with

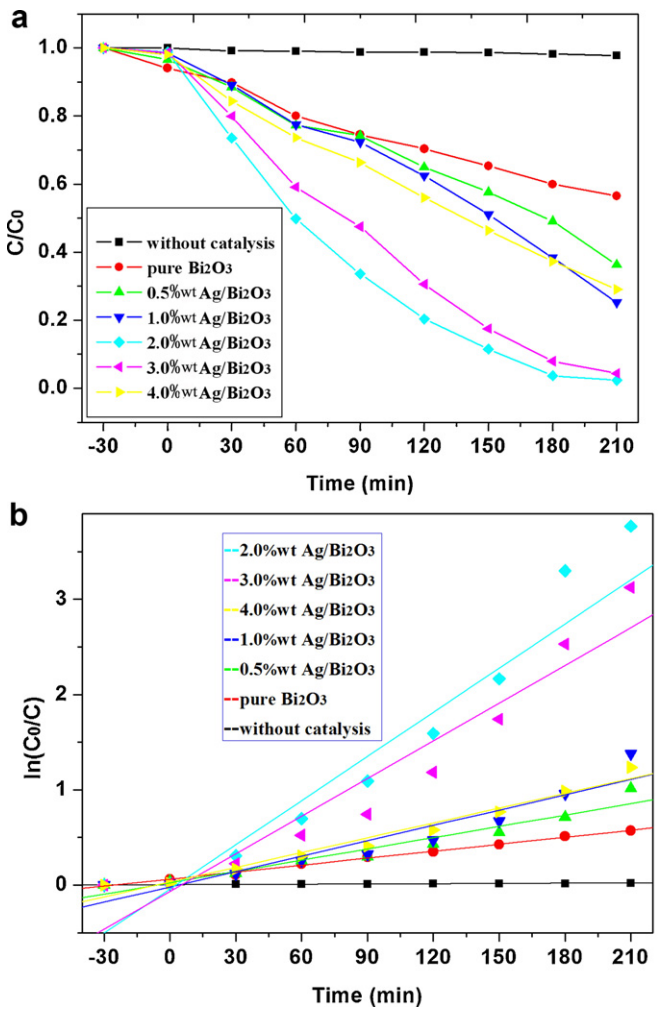

Fig. 10. Photocatalytic activity of Ag/β-Bi_2O_3 samples with different Ag contents.

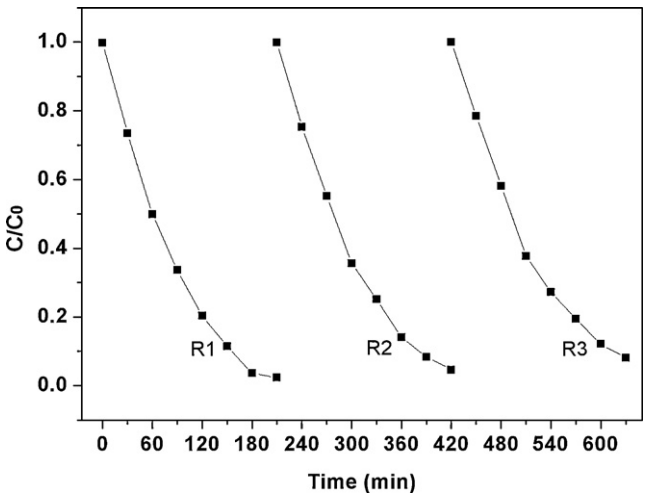

Fig. 11. Recycling experiments for the photodegradation of RhB by Ag/β-Bi_2O_3 sample with 2.0 wt% Ag under visible light irradiation.

2.0 wt% Ag. It should also be noted that the Ag/β-Bi_2O_3 sample with 4.0 wt% Ag content shows a decreased photocatalytic activity.

In order to quantitatively understand the reaction kinetics of the RhB degradation in our experiments, the pseudo-first order is used to fit the experimentally obtained data. The pseudo-first order is expressed as $\ln(C_0/C) = kt$, where C_0 and C are the concentrations of the RhB in aqueous solution at time 0 (the time to obtain adsorption–desorption equilibrium) and t, respectively, and k is the pseudo-first order rate constant. The pseudo-first order rate constant (k) for the as-prepared Ag/β-Bi_2O_3 sample is calculated based on the data plotted in Fig. 10b as a function of Ag content. The calculated pseudo-first order rate constant for the samples can placed in the following sequence according to the Ag content: 0.0054 min^{-1} (2.0 wt%) > 0.0024 min^{-1} (3.0 wt%) > 0.0155 min^{-1} (1.0 wt%) > 0.00088 min^{-1} (4.0 wt%) > 0.0132 min^{-1} (0.5 wt%) > 0.0052 min^{-1} (0 wt%). It is obvious that the presence of Ag nanoparticles in β-Bi_2O_3 accelerates the photodegradation reaction up to 2.0 wt% and then slows with the increase in Ag content.

Above presented results indicate that the photocatalytic activities of the Ag/β-Bi_2O_3 samples are significantly enhanced as the Ag nanoparticles are homogenously distributed on the surface of β-Bi_2O_3 microspheres. Based on the results obtained in the photocatalytic experiments, a photocatalytic mechanism under visible light irradiation can be proposed as follows. As is known, the work function of the Ag is higher than that of the β-Bi_2O_3. Thus, when the Ag gets a contact with the β-Bi_2O_3, a Schottky barrier is formed between them. As the β-Bi_2O_3 microspheres loaded with Ag nanoparticles are illuminated under visible light, the photogenerated electrons in the β-Bi_2O_3 will continuously transfer across the β-Bi_2O_3–Ag interface to the Ag under the effect of the Schottky barrier. Consequently, the recombination of electron and hole is effectively suppressed, more holes can reach the surface of the β-Bi_2O_3 and thus the photocatalytic activity can be greatly enhanced. As more Ag is incorporated into the β-Bi_2O_3, the excess Ag occupies the active sites of the β-Bi_2O_3 surface and thereby reduces the efficiency of the charge separation; therefore, the photocatalytic activity of the Ag/β-Bi_2O_3 sample starts to decrease.

To study the recyclability and photostability of the as-prepared photocatalyst, the Ag/β-Bi_2O_3 sample loaded with 2.0 wt% Ag was collected, dried and reused in three successive photoreaction experiments. Fig. 11 shows the results of the three successive runs of the RhB degradation by Ag/β-Bi_2O_3 sample loaded with 2.0 wt% Ag under visible light irradiation. During these repeated experiments, the experimental conditions, such as pH, initial RhB concentration and ionic strength were kept the same. From Fig. 11, it is found that the as-prepared photocatalyst retains its photocatalytic ability even after three successive runs, each of which lasts for 210 min with 92% removal of the RhB. The obtained results demonstrated that the Ag/β-Bi_2O_3 sample loaded with 2.0 wt% Ag will be a promising photocatalyst for the photodegradation of organic dyes in water.

4. Conclusions

In summary, the visible-light-responsive Ag/β-Bi_2O_3 microspheres were synthesized by a simple chemical method. β-Bi_2O_3 microspheres were obtained by a thermal treatment of sphere-like $Bi_2O_2CO_3$ precursor at 360 °C for 3 h in air and then Ag nanoparticles were in situ incorporated into β-Bi_2O_3 microspheres by impregnation method. The XRD results showed that heat treatment at 360 °C for 3 h was favorable for the complete formation of β-Bi_2O_3 from the $Bi_2O_2CO_3$ precursor. The SEM and TEM observation indicated that the morphology of the $Bi_2O_2CO_3$ precursor was not affected by the phase transformation from $Bi_2O_2CO_3$ to β-Bi_2O_3 and Ag nanoparticles were present on the surface of β-Bi_2O_3. The visible light absorption of β-Bi_2O_3 photocatalyst was greatly enhanced with the incorporation of Ag nanoparticles. The estimated optical band gap of Ag/β-Bi_2O_3 photocatalyst decreased with the increase in Ag content that further influenced photocatalytic activity. The

photocatalytic activity of Ag/β-Bi_2O_3 sample was evaluated by the photodegradation of the Rhodamine-B under visible light irradiation as a function of Ag content. It was found that the photocatalytic efficiency of β-Bi_2O_3 could be significantly improved with the addition of Ag nanoparticles up to 2.0 wt% because the structure of Ag/β-Bi_2O_3 favored the migration of the electron–hole pairs, leading to a higher photocatalytic activity.

Acknowledgments

The present work was supported by the Major Program of the National Natural Science Foundation of China (Grant No. 90923012), the Ministry of Science and Technology of China (Grant No. 2009AA03Z218) and the Research Fund for the Doctoral Program of Higher Education of China (Grant No. 200806980023).

References

[1] M. Inagaki, N. Kondo, R. Nonaka, E. Ito, M. Toyoda, K. Sogabe, T. Tsumura, J. Hazard. Mater. 161 (2009) 1514–1521.
[2] D. Wang, B. Yu, F. Zhou, C. Wang, W. Liu, Mater. Chem. Phys. 113 (2009) 602–606.
[3] Y. Xie, X. Zhao, Y. Li, Q. Zhao, X. Zhou, Q. Yuan, J. Solid State Chem. 181 (2008) 1936–1942.
[4] D. Li, H. Haneda, N.K. Labhsetwar, S. Hishita, N. Ohashi, Chem. Phys. Lett. 401 (2005) 579–584.
[5] G. Shao, J. Phys. Chem. C 112 (2008) 18677–18685.
[6] J. Liu, L. Chang, J. Wang, M. Zhu, W. Zhang, Mater. Sci. Eng. B 172 (2010) 142–145.
[7] A. Cabot, A. Marsal, J. Arbiol, J.R. Morante, Sens. Actuators B 99 (2004) 74–89.
[8] K. Sardar, T.-T. Fang, T.-W. Yang, J. Am. Ceram. Soc. 90 (2007) 4033–4035.
[9] T.P. Gujar, V.R. Shinde, C.D. Lokhande, S.-H. Han, J. Power Sources 161 (2006) 1479–1485.
[10] Y. Qiu, M. Yang, H. Fan, Y. Zuo, Y. Shao, Y. Xu, X. Yang, S. Yang, Cryst. Eng. Commun. 13 (2011) 1843–1850.
[11] K. Brezesinski, R. Ostermann, P. Hartmann, J. Perlich, T. Brezesinski, Chem. Mater. 22 (2010) 3079–3085.
[12] C. Wu, L. Shen, Q. Huang, Y.-C. Zhang, Mater. Lett. 65 (2011) 1134–1136.
[13] L. Zhou, W. Wang, H. Xu, S. Sun, M. Shang, Chem. Eur. J. 15 (2009) 1776–1782.
[14] X. Lin, F. Huang, W. Wang, J. Shi, Scripta Mater. 56 (2007) 189–192.
[15] A. Hameed, V. Gombac, T. Montini, L. Felisari, P. Fornasiero, Chem. Phys. Lett. 483 (2009) 254–261.
[16] M.R. Hoffmann, S.T. Martin, W. Choi, D.W. Bahnemann, Chem. Rev. 95 (1995) 69–96.
[17] L. Yang, C. Hu, Y. Nie, J. Qu, Environ. Sci. Technol. 43 (2009) 2525–2529.
[18] L. Zhao, Z. Sun, J. Ma, H. Liu, Environ. Sci. Technol. 43 (2009) 2047–2053.
[19] P.V. Kamat, D. Meisel, Curr. Opin. Colloid Interface Sci. 7 (2002) 282–287.
[20] J. Geng, F. Wang, Y. Wu, G. Lu, Catal. Lett. 135 (2010) 114–119.
[21] N. Pugazhenthiran, P. Sathishkumar, S. Murugesan, S. Anandan, Chem. Eng. J. 168 (2011) 1227–1233.
[22] S. Anandan, G.-J. Lee, P.-K. Chen, C. Fan, J.J. Wu, Ind. Eng. Chem. Res. 49 (2010) 9729–9737.
[23] Y. Zheng, F. Duan, M. Chen, Y. Xie, J. Mol. Catal. A 317 (2010) 34–40.
[24] M. Wu, B. Yang, Y. Lv, Z. Fu, J. Xu, T. Guo, Y. Zhao, Appl. Surf. Sci. 256 (2010) 7125–7130.
[25] J.-G. Yu, H.-G. Yu, B. Cheng, X.-J. Zhao, J.C. Yu, W.-K. Ho, J. Phys. Chem. B 107 (2003) 13871–13879.
[26] Y. Lai, M. Meng, Y. Yu, Appl. Catal. B 100 (2010) 491–501.